Distribution and Validation of Cloud Cover Derived from AVHRR Data Over the Arctic Ocean During the SHEBA Year

P. Minnis
National Aeronautics and Space Administration
Langley Research Center
Hampton, Virginia

D. A. Spangenberg and V. Chakrapani
Analytical Services and Materials, Inc.
Hampton, Virginia

Introduction

Determination of cloud radiation interactions over large areas of the Arctic is possible only with the use of data from polar orbiting satellites. Cloud detection using satellite data is difficult in the Arctic due to the minimal contrast between clouds and the underlying snow surface in visible and infrared wavelengths. Polar clouds are frequently warmer or at the same brightness temperature as the background surface, complicating cloud detection. The brightness temperature differences between the National Oceanic and Atmospheric Administration (NOAA) advanced very high resolution radiometer (AVHRR) 3.7 and 11-μm channels (BTD34) aid the detection during the day and at night. In strong daylight, the solar-reflected component of the 3.7-μm radiance provides a strong signal of the presence of clouds over snow. At night, the scattering of upwelling radiation from within the cloud at 3.7 μm enables the detection clouds trapped in the surface-based inversion using BTD34. However, at high solar zenith angles (SZA), the solar-reflected component at 3.7 μm is nearly cancelled by the internal scattering by the cloud resulting in a small difference in BTD34 for clear and cloudy scenes. The 12-μm channel, common to many modern satellite imagers, may be valuable for improving cloud detection at large values of SZA.

In previous work, automated cloud detection methods were developed and applied to daytime (Chakrapani et al. 2001, Spangenberg 2001, Trepte et al. 2001) and nighttime (Spangenberg et al. 2002) AVHRR data taken over the Arctic Ocean in the vicinity of the Surface Heat Budget of the Arctic Ocean (SHEBA) ship. The ARM-sponsored cloud radar data on the SHEBA ship were used to validate the cloud detection. In this study, an enhanced AVHRR polar cloud mask is used to discriminate between clouds and the background surface over the SHEBA ship and surrounding domain for daytime, nighttime, and twilight scenes between January and September 1998. The satellite-derived cloud amounts are validated by comparing them to cloud radar, lidar, and AVHRR Polar Pathfinder (APP) data (Maslanik et al. 1997). Monthly-mean cloud amount, height, and cloud radiative forcing values are computed in the immediate vicinity of the SHEBA ship and over a larger domain in the western Arctic

Ocean. This improved methodology provides the basis for routine analyses of AVHRR data over the ARM North Slope of Alaska (NSA) domain.

Data

NOAA-12 and 14 AVHRR 1-km data that encompass the SHEBA ship and surrounding area are used here. These data are taken from approximately 275-335 orbits for any given month of 1998. NOAA-12 and 14 sample all hours of the day except 20-24 local time (LT). The cloud detection algorithm, or mask, classifies, as clear or cloudy, each pixel within a circular area defined by a 25-km radius centered on the SHEBA ship and over an 8° latitude by 32° longitude domain divided into a 56 x 56 km^2 regional grid. Figure 1 shows the ship track and regional analysis grid.

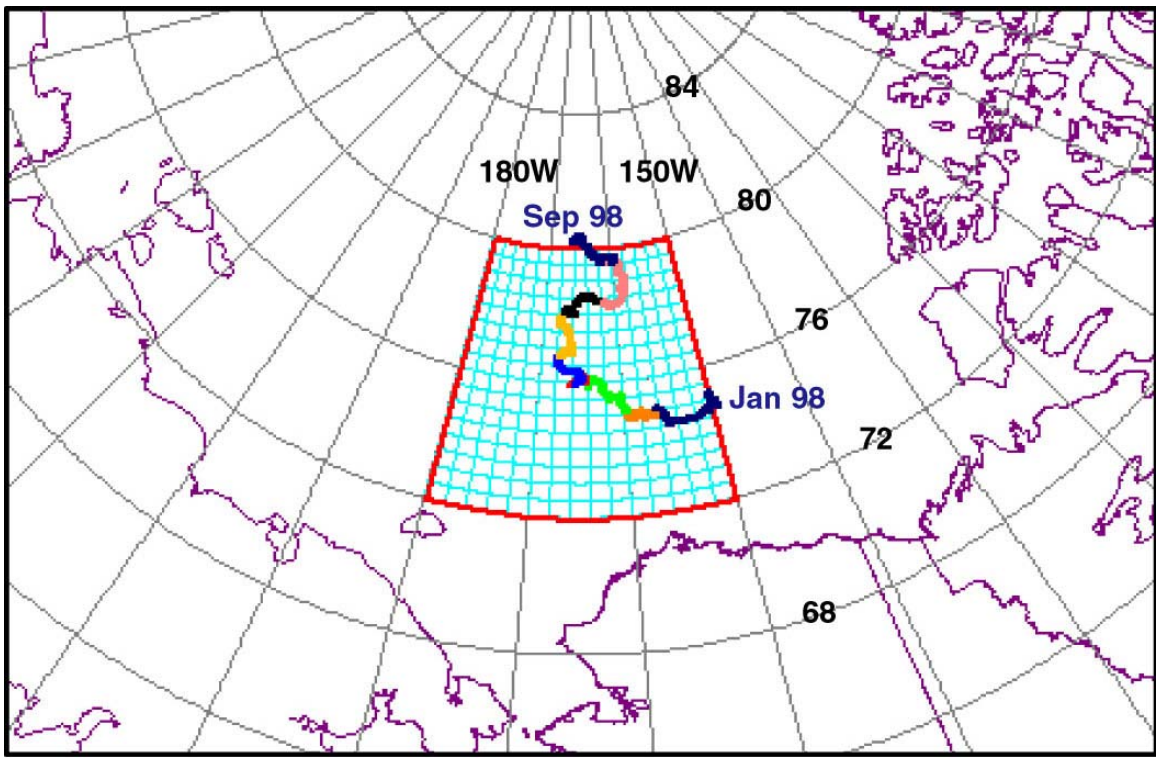

Figure 1. SHEBA ship track and analysis domain. Grid boxes are 0.5° latitude by 2.0° longitude.

AVHRR 0.65-µm reflectance (R_{06}), and the 3.7, 11, and 12-µm brightness temperatures, T3, T4, and T5, respectively, are used in the analysis. To remove noise from the AVHRR 3.7-µm band at low temperatures, we used the parametric Wiener filter technique of Simpson and Yhann (1994). The filter works best at night when the T3 and T4 images have similar patterns.

European Center for Medium-Range Weather Forecasting (ECMWF) profiles were used to specify the vertical temperature and humidity profiles used to account for atmospheric absorption and to convert the cloud temperature Tc to cloud height z. The ECMWF skin temperatures were used to predict the clear-sky brightness temperature at 11 µm for use in the cloud mask. The correlated k-distribution method of

Kratz (1995) was used to convert surface temperature to clear-sky background brightness temperatures. Other input data include snow and ice maps from the National Snow and Ice Data Center and clear-sky albedo (Sun-Mack et al. 1999) and surface emittance (Chen et al. 2002) maps developed for the Cloud's and the Earth's Radiant Energy System (CERES) Project.

Cloud Mask

During daytime (SZA >82°), the cloud mask uses theoretical 3.7-μm reflectance models over snow (Spangenberg et al. 2001), along with the CERES polar mask framework (Trepte et al. 2001) developed for the Terra moderate resolution imaging spectroradiometer (MODIS). The daytime mask compares the reflected part of the T3 radiance (R_{37}) with the clear-sky snow model value to discriminate clear-sky from snow-covered surfaces. The variability in clear-sky R_{37} was obtained from the subjective cloud mask of Minnis et al. (2001) that was applied during the May-July 1998 intensive observation period. During the melt season, R_{06}, R_{37}, and T4 threshold tests are used to supplement the R_{37} snow model test. Detecting daytime Arctic haze from otherwise clear pixels is accomplished by flagging high values (>0.7 K) of the brightness temperature difference BTD45 between T4 and T5.

For nighttime (SZA >91°) and twilight (82° <SZA <91°) scenes, cloud amounts are determined strictly from the temperature threshold approach of Spangenberg et al. (2002). Many of the polar nocturnal clouds are detected with the BTD34 test for clouds trapped in the relatively warm inversion layer. These clouds have temperatures greater than the background snow surface with relatively low, often negative, BTD34 values. Clouds above the Arctic inversion are detected at night using BTD34, BTD45, and an estimate of the upper-level relative humidity from the ECMWF model. These higher clouds typically have relatively large BTD34 and BTD45 values with temperatures at or below that of the underlying snow surface. For twilight periods, the nighttime algorithm was modified to account for weak solar radiation reflecting from the cloud tops. Also, because of the relatively high R_{37} for forward scattering at large viewing zenith angles, a special set of twilight tests is applied for this viewing geometry. Because of the difficulty in classifying pixels as clear or cloudy at night, weak clear and weak cloud categories are defined. The weak categories are likely to contain Arctic haze, thin cirrus, steam fog, or diamond dust.

Validation

The AVHRR-derived cloud amounts from the polar mask are validated by comparison with NOAA Environmental Technology Laboratory (ETL) millimeter-wave cloud radar (MMCR) cloud amounts. NOAA-ETL depolarization and backscatter unattended lidar (DABUL) data were used to confirm the MMCR cloud amounts. If the radar and lidar disagreed, the corresponding satellite image was excluded from the comparison. The satellite cloud amounts were computed by averaging all the cloud mask pixels falling within a 25-km radius centered on the SHEBA ship. MMCR cloud amounts were computed as 20-minute time averages of cloud boundary data centered at the satellite overpass times. Monthly-mean cloud amounts from the radar and polar cloud mask, including root-mean-squared (rms) errors, are shown in Figure 2. In this particular comparison, weak clear or weak cloud amounts over the SHEBA ship exceeding 10% were excluded; this represents roughly 10-30% of the nighttime orbits. For strong radar cloud signals with reflectances above -20 dBZ, the satellite cloud amounts were 88-100% in

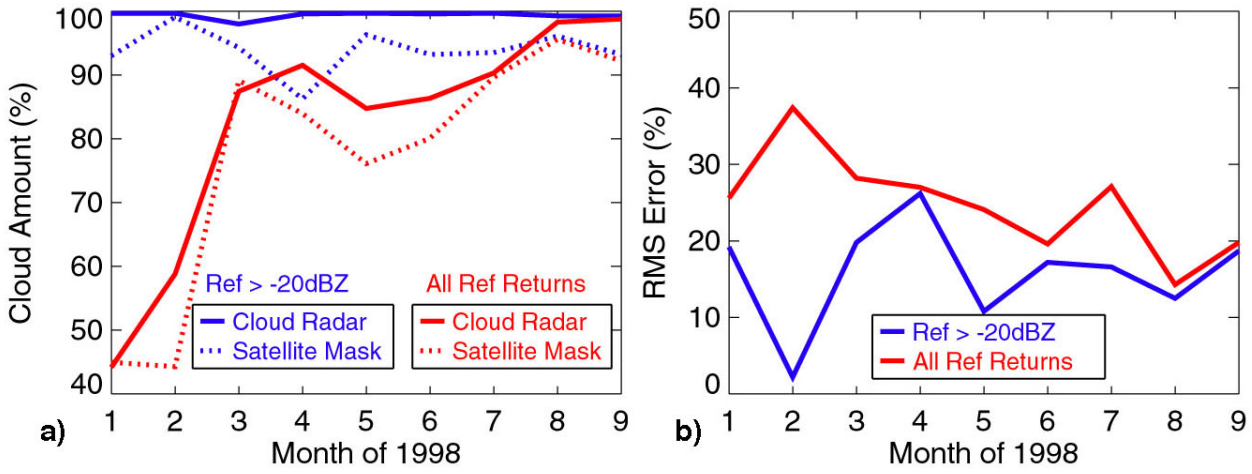

Figure 2. January-September 1998 AVHRR cloud cover validation at SHEBA using MMCR data. a) Cloud amounts and b) rms errors.

all months. The rms errors are lowest for the strong cloud case, ranging from 2% in February to 26% in March. For the all radar reflectance returns case, the satellite cloud amounts are generally within 10% of the radar. However, cloud amounts were underestimated by 15% in February with a high rms error. This is likely due to the abundance of thin cirrus clouds, which showed little or no signal in the satellite imagery. The ground-based cloud radar is tuned to see all types of thin clouds, while the satellite cloud detection threshold is less sensitive, especially over cold snow surfaces. The best overall agreement between the cloud mask and radar occurred during the summer months. This is to be expected because it is easiest to detect clouds during perpetual daylight over dark melt ponds and open ocean surfaces.

The performance of the ARM AVHRR (AA) polar mask was further assessed by comparing the cloud amount output with cloud coverage from a polar mask used by the AVHRR Polar Pathfinder project (Maslanik et al. 1997). The APP cloud amount product is derived from the Cloud and Surface Parameter Retrieval (CASPR) system of Key (2000). Figure 3 shows a comparison between the MMCR, AA, and APP monthly-mean cloud amounts over the SHEBA site. The solid lines are for one orbit per day, centered at 14:00 LT. Only orbits having coincident APP and MMCR data were used. Cloud cover increases significantly from winter to summer in the MMCR and AA cloud amounts. APP cloud amounts are fairly constant around 70%. The APP overestimates cloud cover at night and slightly underestimates it during the daytime compared to the cloud radar. The AA cloud amounts show somewhat better agreement in capturing the increasing cloud trend observed in the MMCR. In all months except March, the AA monthly-mean cloud amounts underestimate those of the cloud radar. March has cases of ground fog that is too low to be seen by the upward-looking cloud radar. The “true” cloud amount trend is shown by the dotted lines since this case represents all NOAA-12 and 14 orbits passing over SHEBA. The cloud amount distributions for MMCR, AA, and APP are shown in Figure 4. For nighttime and twilight images in Figure 4a, the cloud amount distribution from the AA mask agrees well with the surface-based MMCR. The APP cloud mask fails to completely capture the clear-sky conditions with the cloud amounts dropping to no more than 25% at night. For the daytime images in Figure 4b, the AA and APP cloud masks do equally well compared to the cloud radar. Some of the apparent underestimate in clear-sky conditions by the AA polar mask during daytime happens because

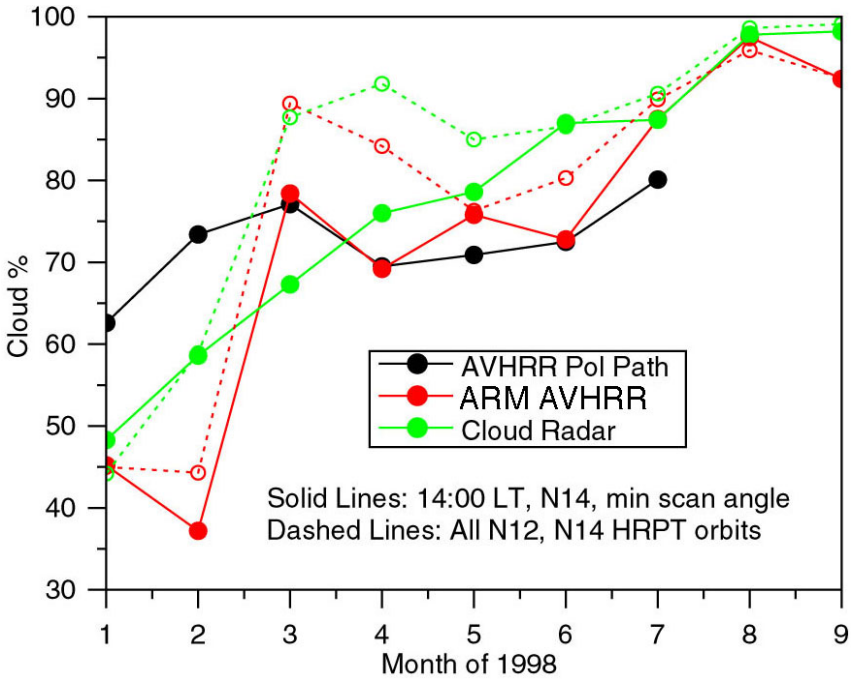

Figure 3. MMCR, ARM-AVHRR, and APP monthly-mean cloud amounts for January-September 1998. All Cloud amounts are for a 25-km radius surrounding the SHEBA ship.

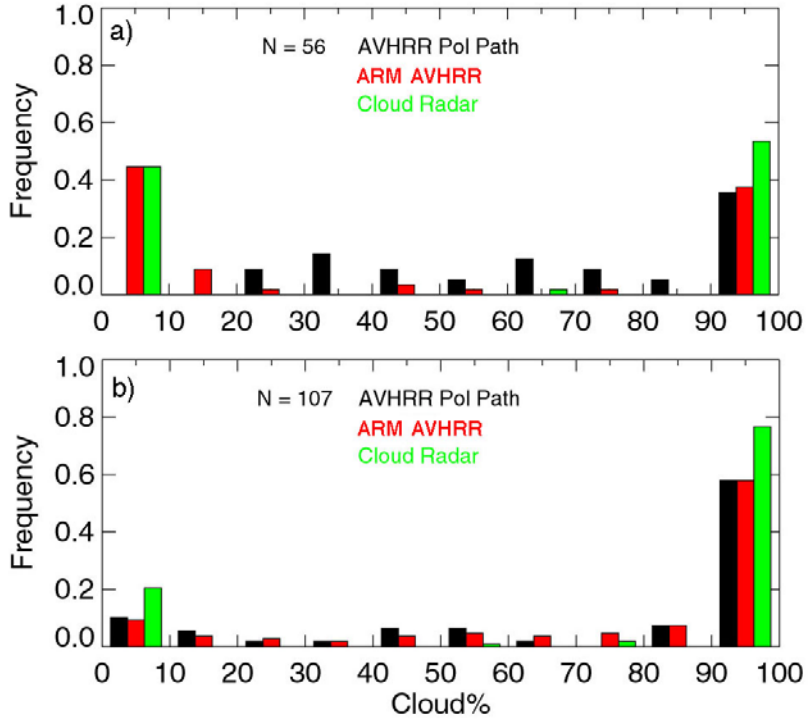

Figure 4. January-July 1998 cloud frequency distribution from MMCR, ARM-AVHRR, and APP. All cloud amounts are for a 25-km radius surrounding the SHEBA site. a) Is for nighttime and twilight combined, while b) is for daytime.

AVHRR can detect steam fog that forms right at the surface. High relative humidity coupled with strong temperature differences between the ambient air and the melt ponds or leads is what causes this type of fog. This steam fog is often too low to be detected by the MMCR.

Results

Monthly-mean cloud amounts, heights, and the top of the atmosphere (TOA) cloud radiative forcing were derived using the time and space averaging method of Young et al. (1998). Values were computed both over the regional grid (Figure 1) and the circle surrounding the SHEBA ship. Cloud-top heights were computed by finding the lowest altitude in the ECMWF temperature soundings where T(z) = T4. Because no correction is applied for semi-transparent clouds, the cloud height may be underestimated for thin clouds.

The AVHRR values of R_{06} and T4 fluxes were converted into broadband shortwave (SW) and longwave (LW) fluxes using the empirical method of Doelling et al. (2001). The latter matched Earth Radiation Budget Experiment (ERBE) and NOAA-9 AVHRR data from 1986 to obtain the empirical regression fits. The respective TOA cloud radiative forcings for SW, LW, and net radiation are

$$SWCRF = M_{SWCLR} - M_{SW} \quad (1)$$

$$LWCRF = M_{LWCLR} - M_{LW} \quad (2)$$

$$NETCRF = SWCRF + LWCRF, \quad (3)$$

where M is the flux and the subscript CLR refers to clear-sky conditions. The monthly-hourly mean diurnal SW, LW, and net cloud forcing for the seasonal months of January, April, July, and September 1998 are shown in Figure 5. SWCRF in Figure 5a is 0 Wm^{-2} in January with values peaking near -60 Wm^{-2} in July when the surface is dark and the sun is high. SWCRF is also larger for the greater incoming solar flux centered at local noon. During April SWCRF increases to -10 Wm^{-2}, indicating that the clouds added only a bit more reflectance to that of the background snow surface. Positive LWCRF in Figure 5b is most pronounced in July and September, with values around 10 Wm^{-2}. This indicates the presence of clouds mostly colder that the surface. Conversely, LWCRF is slightly less than zero in January, indicating that clouds are mostly warmer than the cold snow surface. Because of the snow, ice, or ocean surface, minimal diurnal variability is seen in the LWCRF in Figure 5b. In the LW, as winter changes to summer, clouds shift from having a cooling effect on the earth-atmosphere system to having a warming one. NETCRF in Figure 5c equals LWCRF in January, with values around -3 Wm^{-2}. Over the course of a day during April, a net loss of 0 to 10 Wm^{-2} of energy results from the cloud cover. NETCRF reaches a minimum at local noon during July, with values at -50 Wm^{-2}. During all seasons examined here, clouds acted to cool the earth-atmosphere system over the Arctic with the exception of the autumn night. The SHEBA cloud forcing values have the same trends as the regional grid with the greatest differences occurring in July.

The cloud amount, height, and cloud forcing distribution over the regional grid for the four seasonal months of 1998 are shown in Figure 6. Large gradients in cloud amount of 30%-50% can be seen across the regional grid, probably reflecting the strength of subsidence from Arctic high pressure in the cold

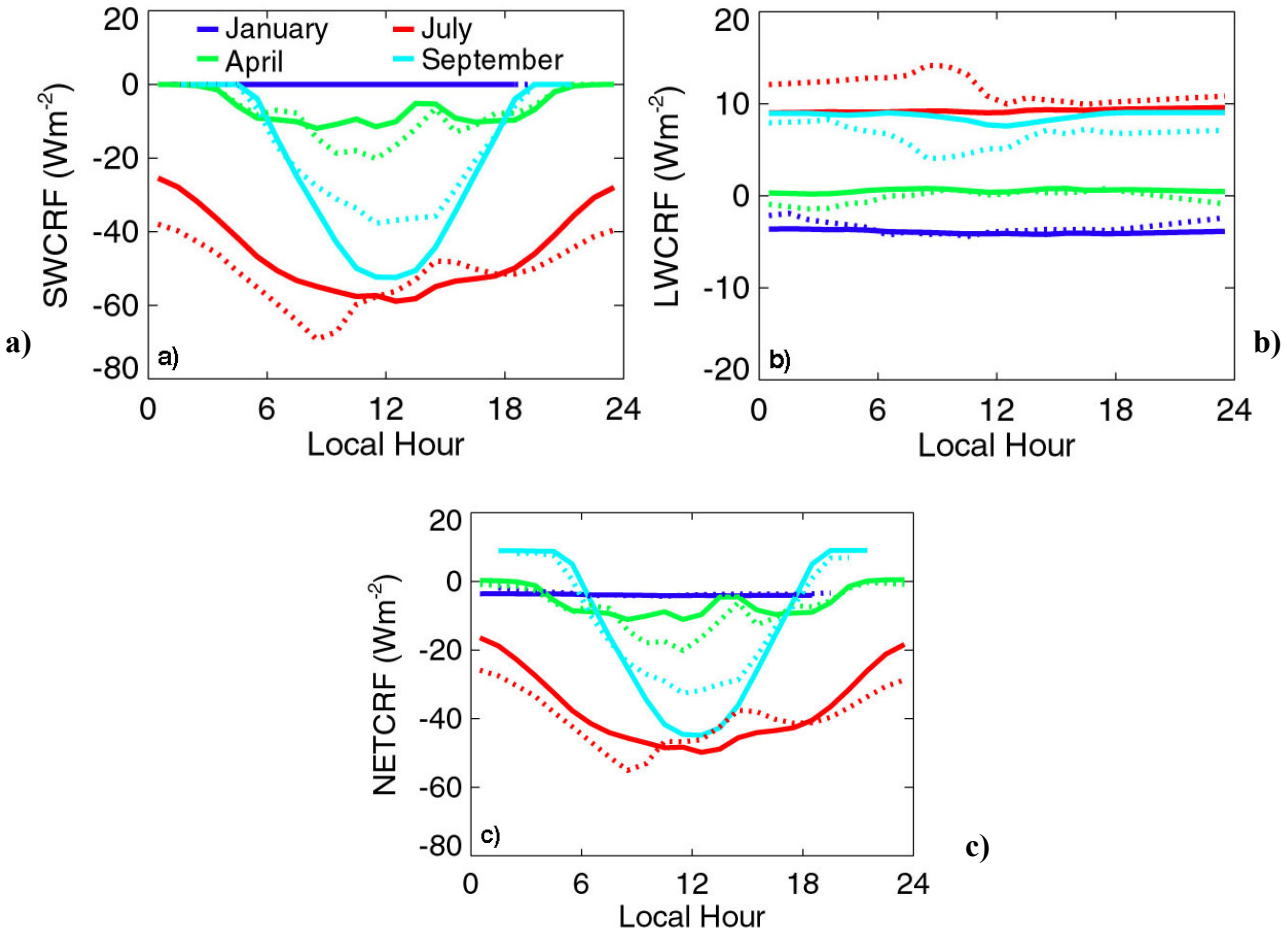

Figure 5. Mean hourly TOA cloud radiative forcing for SHEBA. Solid lines are for the regional grid and dashed lines are for the 25-km radius. a) SW cloud forcing, b) LW forcing, and c) net forcing.

season and the storm track in the melt season. The cloud amounts ranged from 30% in January over the northeast corner of the grid to 100% over central areas in September. The cloud heights show the greatest change across the domain during July, with the storm track likely passing through the area of maximum cloudiness. A maximum cloud height of 4 km occurred over the northern part of the grid in July near the SHEBA site. This maximum in cloud height is likely resulting from strong storm systems. The mean NETCRF varies little over the domain during January and April but changes by 20 Wm^{-2} or more across the area in July and September. This large spatial variability in NETCRF occurred because of the different surface conditions and cloud types existing over the domain in those months. The cloud forcing values are mostly between 0 and -10 Wm^{-2} in all seasons except during summer when values were commonly down to -40 Wm^{-2}.

Conclusions and Future Work

A polar cloud mask was developed for NOAA-AVHRR to include day, night, and twilight viewing conditions. The daytime algorithm uses 3.7-µm reflectance models over snow, while the nighttime and

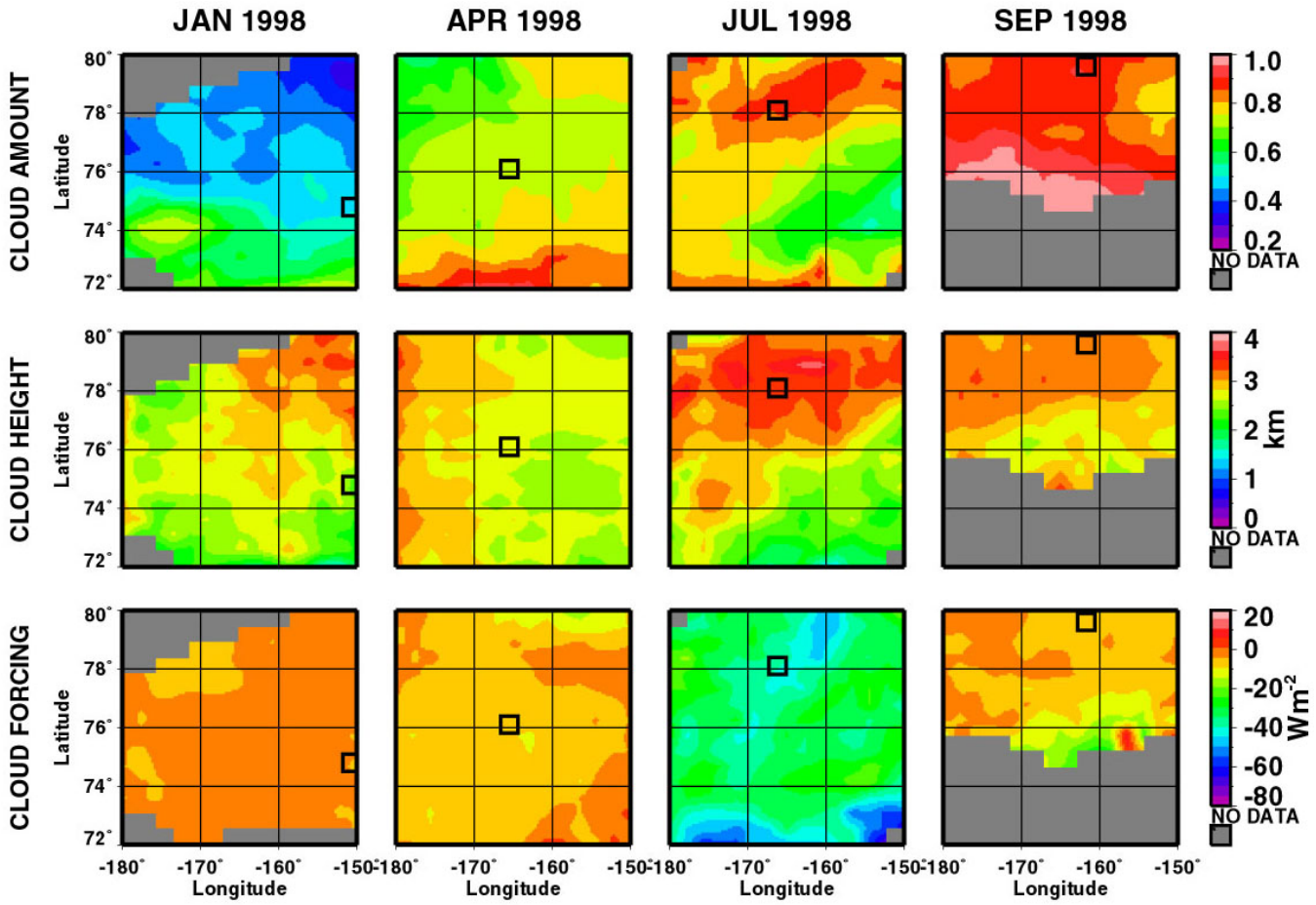

Figure 6. Cloud amount, height, and TOA net cloud radiative forcing distributions over the regional grid for January, April, July, and September 1998. The square marks the SHEBA ship location.

twilight algorithms are based on a brightness temperature threshold approach. The ARM-AVHRR polar cloud mask captured most of the clouds seen in the radar and lidar, with rms errors between 14 and 37%. Much of the rms error resulted from the inability of the AVHRR to detect very thin cirrus over cold snow surfaces. Since this type of cloud does not significantly alter the Arctic radiation balance, the misclassification of the cloudy cirrus pixels as clear-sky should have minimal impact on Arctic climate studies. Another source of rms error came from the ground-based sensors missing very low-lying steam fog that appeared in the satellite imagery. Compared to the MMCR cloud amounts over SHEBA, the ARM-AVHRR polar mask is generally closer than the APP at night and similar to it during the day. Cloud amounts significantly increased from winter to late summer over the SHEBA site during 1998, with values ranging from 40 to 95%. The ship was located in an area of particularly high cloudiness in July compared to areas further south and east. Mean cloud heights over the western Arctic Ocean were nearly constant from winter to summer, with values ranging from 2 to 4 km. Overall, clouds caused the planet to cool during all seasons examined, with cooling most pronounced during the melt season. Over the seasons, the mean diurnal cloud forcing ranged from 10 Wm^{-2} in fall at night to -50 Wm^{-2} in summertime at local noon.

The cloud mask will be applied to data from more recent years over the ARM NSA site with new broadband fluxes derived from matched CERES broadband and Terra-MODIS narrowband data. Cloud products including optical depth, phase, emittance, ice diameter, and ice water path will also be made available. Polar radiation and cloud data can be found on our web page at: http://www-pm.larc.nasa.gov/arm/NSA/arm-nsa.html.

Corresponding Author

Patrick Minnis, p.minnis@nasa.gov, (757) 864-5671.

Acknowledgements

This research was supported by the Environmental Sciences Division of U.S. Department of Energy Interagency Agreement DE-AI02-97ER62341 under the Atmospheric Radiation Measurement Program. We would like to thank Taneil Uttal and NOAA-ETL for providing the SHEBA cloud radar data used in this study. Also, Jeff Key and the Polar Satellite Meteorology Group at the University of Wisconsin for providing the SHEBA-CASPR cloud dataset.

References

Chakrapani, V., D. A. Spangenberg, D. R. Doelling, P. Minnis, Q. Z. Trepte, and R. F. Arduini, 2001: Improvements in AVHRR daytime cloud detection over the ARM NSA Site. . In *Proceedings of the Eleventh Atmospheric Radiation Measurement (ARM) Science Team Meeting*, ARM-CONF-2001. U.S. Department of Energy, Washington, D.C. Available URL: http://www.arm.gov/docs/documents/technical/conf_0103/chakrapani-v.pdf

Chen, Y., S. Sun-Mack, P. Minnis, D. F. Young, and W. L. Smith, Jr., 2002: Surface spectral emissivity derived from MODIS data. *Proc. SPIE 3rd Intl. Asia-Pacific Environ. Remote Sensing Symp. 2002: Remote Sens. of Atmosphere, Ocean, Environment, and Space*, October 23-27, Hangzhou, China.

Doelling, D. R., P. Minnis, D. A. Spangenberg, V. Chakrapani, A. Mahesh, F. P. J. Valero, and S. Pope, 2001: Cloud radiative forcing at the top of the atmosphere during FIRE-ACE derived from AVHRR data. *J. Geophys. Res.*, **106**, 15,279-15,296.

Key, J, 2000: The cloud and surface parameter retrieval (CASPR) system for polar AVHRR. Cooperative Institute for Meteorological Satellite Studies, p. 59, University of Wisconsin, Madison.

Kratz, D. P., 1995: The correlated k-distribution technique as applied to the AVHRR channels. *J. Quant. Spectrosc. Radiative Transfer*, **53**, 501-517.

Maslanik, J., C. Fowler, J. Key, T. Scambos, T. Hutchinson, and W. Emery, 1997: AVHRR-based polar pathfinder products for modeling applications. *Ann. Glaciol.*, **35**, 171-182.

Minnis, P., D. R. Doelling, V. Chakrapani, D. A. Spangenberg, L. Nguyen, R. Palikonda, T. Uttal, M. Shupe, and R. F. Arduini, 2001: Cloud coverage and height during FIRE-ACE derived from AVHRR data. *J. Geophys. Res.*, **106**, 15,215-15,232.

Simpson, J. J. and S. R. Yhann, 1994: Reduction of noise in AVHRR channel-3 Data with minimum distortion. *IEEE Trans. Geosc. and Remote Sens.*, **32**, 315-328.

Spangenberg, D. A., V. Chakrapani, D. R. Doelling, P. Minnis, and R. F. Arduini, 2001: Development of an automated Arctic cloud mask using clear-sky satellite observations taken over the SHEBA and ARM-NSA sites. *Proc. AMS 6th Conf. On Polar Meteorology and Oceanography*, May 14-18, San Diego, California.

Spangenberg, D. A., D. R. Doelling, V. Chakrapani, P. Minnis, and T. Uttal, 2002: Nighttime cloud detection over the Arctic using AVHRR data. In *Proceedings of the Twelfth Atmospheric Radiation Measurement (ARM) Science Team Meeting*, ARM-CONF-2002. U.S. Department of Energy, Washington, D.C.

Sun-Mack, S., Y. Chen, T. D. Murray, P. Minnis, and D. F. Young, 1999: Visible clear-sky and near-infrared surface albedos derived from VIRS for CERES. In *Proceedings of the Tenth Atmospheric Radiation Measurement (ARM) Science Team Meeting,* U.S. Department of Energy, Washington, D.C.

Trepte, Q., R. F. Arduini, Y. Chen, S. Sun-Mack, P. Minnis, D. A. Spangenberg, and D. R. Doelling, 2001: Development of a daytime polar cloud mask using theoretical models of near-infrared bi-directional reflectance for ARM and CERES. *Proc. AMS 6th Conf. On Polar Meteorology and Oceanography*, May 14-18, San Diego, California.

Young, D. F., P. Minnis, G. G. Gibson, D. R. Doelling, and T. Wong, 1998: Temporal interpolation methods for the Cloud's and the Earth's Radiant Energy System (CERES) Experiment. *J. Appl. Meteorol*., **37**, 572-590.